The structure design of Poly(ester imide)s with low dielectric loss and high mechanical properties

Chenggang Zhang[a], Xiaojie He[a], Qinghua Lu[*b]

a. School of Chemical Science and Technology, Tongji University, Siping Road No. 1239, Shanghai, 200092, China

b. Shanghai Key Lab of Electrical & Thermal Aging, the State Key Laboratory of Metal Matrix Composites, School of Chemistry and Chemical Engineering, Shanghai Jiao Tong University, Dongchuan Road No. 800, Shanghai, 200240, China

Corresponding Author

* E-mail: qhlu@sjtu.edu.cn (Q.Lu).

Contents

1. Experimental details

1.1 Synthesis of monomers

1.2 Computational simulations

1.3 Crystallinity calculation

2. Figures and tables

Table S1. Humidity provided by the saturated solution at 25 °C.

Table S2. Molecular Weights and PDIs of PAAs.

Table S3. Crystallization of PEsEtIs.

Table S4. MD results for PEsEtIs.

Table S5. Polarity for PEsEtIs.

Figure S1. Synthetic route of TA2EN.

Figure S2. ^{1}H-NMR spectrum of TA2EN in DMSO-d_6.

Figure S3. The images of PEsEtI films.

Figure S4. FTIR spectra of A2EB-ODA-TA2EN (a) and A2EB-ODA-TA2EB (b).

Figure S5. Peak fitting of PEsEtIs.

Figure S6. The POM images of PEsEtIs.

Figure S7. Three-dimensional periodic boundary cells of PEsEtI films.

Figure S8. DMA curves of PEsEtIs.

Figure S9. DSC curves of PEsEtIs.

Figure S10. TGA curves of PEsEtIs.

Figure S11. TMA curves of PEsEtIs.

Figure S12. Stress-strain curves of PEsEtIs.

1. Experimental details

1.1 Synthesis of monomers

The synthetic route for TA2EN is shown in **Figure S1** [1]. 2,6-dihydroxynaphthalene (HO-1N) was dissolved in THF in the presence of pyridine as an HCl acceptor and trimellitic anhydride chloride (TAC) was dissolved in THF in flasks sealed with a septum cap. The HO-1N solution was added to the TAC solution at 0 °C slowly using a syringe with continuous magnetic stirring, after which the reaction mixture was stirred at room temperature for 12 h. The formed crude product was collected by filtration, washed with a small quantity of THF and a large quantity of Ethyl alcohol and ethyl acetate, and then dried at 80 °C for 24 h. The crude product was purified by refluxing with acetic anhydride at 80 °C, followed by filtration. The resulting precipitate was washed with ethanol and ethyl acetate, and dried under vacuum at 120 °C for 24 hours to yield the final product, TA2EN. The ^{1}H NMR spectra of TA2EN is shown in Figure S2. TA2EN ^{1}H NMR (400 MHz, DMSO-d6, δ (ppm))：δ 8.46 (s, 2H), 8.38 (d, J = 8.4 Hz,2H), 8.08(d, J = 8.8 Hz, 2H), 8.00 (s, 2H), 7.88 (d, J = 8.0 Hz, 2H), 7.60 (d, J = 10.8 Hz, 2H).

1.2 Computational simulations

The radius of gyration (Rg) represents the root mean square distance of each molecule from its center of mass. The radius of gyration was calculated as:

$$R_g^2 = \frac{\sum_{i=1}^{N} m_i r_i^2}{\sum_{i=1}^{N} m_i} \tag{1}$$

where r_i (Å) is the distance from each atom to the center of mass, m_i (g) is the mass of atom i and N is the number of atoms [2].

The cohesive energy density (CED) refers to the energy required for gasification per mole of material per unit volume to overcome intermolecular forces, which includes the van der Waals CED and electrostatic CED [3].

The adequate measure of conformational rigidity is the value of the Kuhn segment parameter:

$$A_{\text{fr}} = \lim_{n \to \infty} \left(\frac{\langle h^2 \rangle}{n l_0} \right) \tag{2}$$

where h^2 is the mean square distance between the chain ends, n is the number of the repeat units and l_0 is the contour length of the repeat unit [4].

The fractional free volume (FFV) is defined as the specific volume of the membrane matrix divided by the free volume. The Atom Volumes & Surfaces module of MS was employed to generate various surfaces. The FFV of the simulation boxes was calculated as:

$$FFV = \frac{V - V_0}{V} \tag{3}$$

$$V_0 = 1.3 \times V_W \tag{4}$$

where V represents the volume of simulation box, the volume of a van der Waals system is denoted by V_W and an indication of V_0 signifies the volume that the polymer chain occupies [5].

The quantum chemical calculations were performed by means of the Gaussian09W [6]

computational package in the frame of DFT. The 6-31G(d) basis sets were adopted together with

the hybrid B3LYP functional. The dipole moment and linear molecular polarizability were

calculated by means of this functional, which combines the three parameters exchange functional

by Becke with the LYP correlation one [7-9].

1.3 Crystallinity calculation.

The crystallinity (X_c) was calculated as [10, 11]:

$$X_c = \frac{A_c}{A_{all}} \times 100\%$$

(5)

where A_c and A_{all} are the crystallization and all peak areas, respectively.

d-spacings of the polyimides were derived from their diffraction peaks by Bragg's law [12]:

$$2d\sin\theta = n\lambda$$

(6)

where d represents the interplanar spacing (d-spacings), n is the diffraction order (generally fixed at 1), the X-ray wavelength λ was 0.15405 nm and θ denote the full width at half peak maximum and Bragg angle, respectively.

The crystallite size of the polyimides was calculated by the Scherrer equation [13]:

$$L = \frac{k\lambda}{\beta\cos\theta}$$

(7)

where L represents the crystallite size, k is the Scherrer constant (generally fixed at 0.89), the X-ray wavelength λ was 0.15405 nm and β and θ denote the full width at half peak maximum and Bragg angle, respectively.

Table S1. Humidity provided by the saturated solution at 25 °C [14, 15].

Saturated Solution	Theoretical humidity (%)	Actual humidity (%)
K_2CO_3	32.78±0.16	42.3
Normal environment	-	53.1
NaBr	57.57±0.40	61.2
NaCl	75.29±0.13	76.8
KBr	80.89±0.21	82.2
K_2SO_4	97.30±0.40	92.3

Table S2. Molecular Weights and PDIs of PAAs.

PEsEtIs	M_n ($\times 10^4$)	M_w ($\times 10^4$)	PDI
ODA-TA2EB	3.08	5.69	1.85
A2EB50-ODA50-TA2EB	3.09	5.25	1.70
A2EB65-ODA35-TA2EB	2.44	4.63	1.90
A2EB75-ODA25-TA2EB	1.66	2.54	1.53
A2EB85-ODA15-TA2EB	1.54	2.37	1.54
A2EB90-ODA10-TA2EB	1.47	2.19	1.49
A2EB-TA2EB	2.16	3.33	1.54
ODA-TA2EN	2.58	3.95	1.53
A2EB50-ODA50-TA2EN	2.16	3.45	1.60
A2EB65-ODA35-TA2EN	2.03	3.28	1.62
A2EB75-ODA25-TA2EN	1.92	3.13	1.63
A2EB85-ODA15-TA2EN	1.72	2.88	1.67
A2EB-TA2EN	2.23	3.70	1.66

Table S3. Crystallization of PEsEtIs.

PI	Crystallinity (%)	2θ (º)	β (º)	L (nm)	d-spacing (nm)
ODA-TA2EB	20	18.91	0.92	8.66	4.69
		22.75	0.96	8.35	3.91
A2EB50-ODA50-TA2EB	24	19.39	1.60	4.96	4.57
		21.41	2.28	3.50	4.15
A2EB65-ODA35-TA2EB	27	19.68	1.70	4.70	4.50
		21.47	2.40	3.34	4.14
A2EB75-ODA25-TA2EB	31	19.68	1.67	4.78	4.51
		21.46	2.39	3.34	4.14
A2EB85-ODA15-TA2EB	31	19.49	1.23	6.50	4.55
		20.57	3.21	2.49	4.31
A2EB90-ODA10-TA2EB	28	20.16	3.00	2.66	4.40
A2EB-TA2EB	32	20.86	3.32	2.54	4.25
ODA-TA2EN	20	18.19	1.48	5.35	4.87
		22.66	1.46	5.48	3.92
		27.21	1.93	4.19	3.27
A2EB50-ODA50-TA2EN	21	19.10	2.14	3.73	4.64
		21.57	2.05	3.90	4.12
A2EB65-ODA35-TA2EN	26	18.82	1.55	5.14	4.71
		20.87	3.18	2.51	4.25
A2EB75-ODA25-TA2EN	27	19.13	2.00	3.98	4.63
		21.31	2.35	3.39	4.17
A2EB85-ODA15-TA2EN	27	19.10	1.80	4.43	4.64

		21.23	2.46	3.24	4.18
		19.22	1.92	4.48	4.61
A2EB-TA2EN	31				
		21.27	1.52	3.18	4.17

Table S4. MD results for PEsEtIs.

CoPEsIs	R_g [a] (Å)	A_{fr} [b] (Å)	CED [c] (J cm^{-3})	FFV [d] (%)
ODA-TA2EB	46.66	3.95	502.6	18.37
A2EB50-ODA50-TA2EB	36.35	2.26	504.7	17.93
A2EB70-ODA30-TA2EB	36.08	2.15	515.4	17.42
A2EB80-ODA20-TA2EB	43.29	2.95	501.9	18.62
A2EB-TA2EB	53.23	6.23	490.6	18.52
ODA-TA2EN	46.93	3.05	486.5	19.63
A2EB50-ODA50-TA2EN	37.6	1.95	493.8	19.01
A2EB70-ODA30-TA2EN	37.5	2.12	507.0	17.63
A2EB80-ODA20-TA2EN	37.46	1.88	511.7	16.89
A2EB-TA2EN	76.77	8.70	509.6	18.32

[a] Radius of gyration; [b] Kuhn segment length; [c] Cohesive energy density; [d] Fractional free volume, FFV = (V-1.3 V_W)/V.

Table S5. Polarity for PEsEtIs.

PI	Dipole moment (D)	α/V [a] (a.u. $\times$ mol cm^{-3})
ODA-TA2EB	2.26	1.029
ODA-TA2EN	1.14	1.019
A2EB-TA2EB	3.12	0.973
A2EB-TA2EN	2.23	1.028

[a] Volume polarizability.
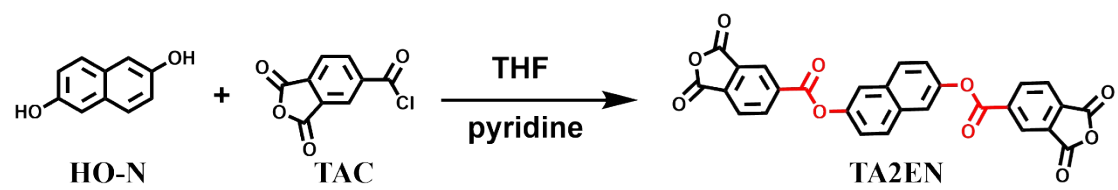
Figure S1. Synthetic route of TA2EN.
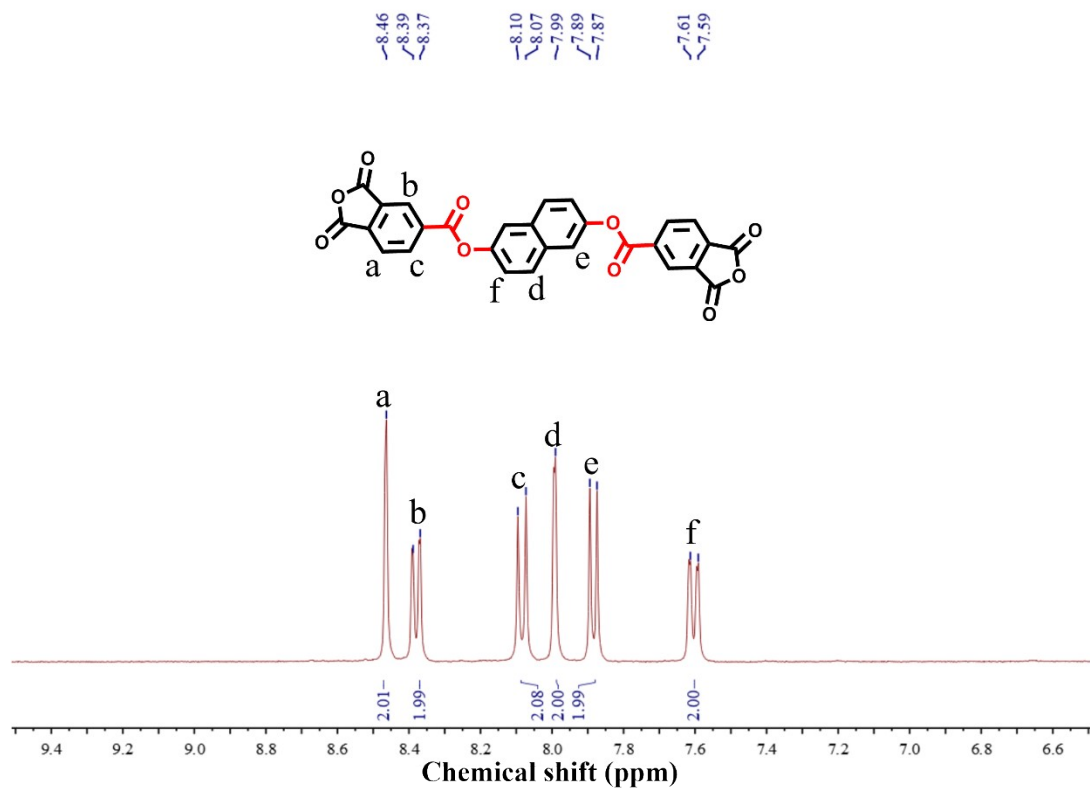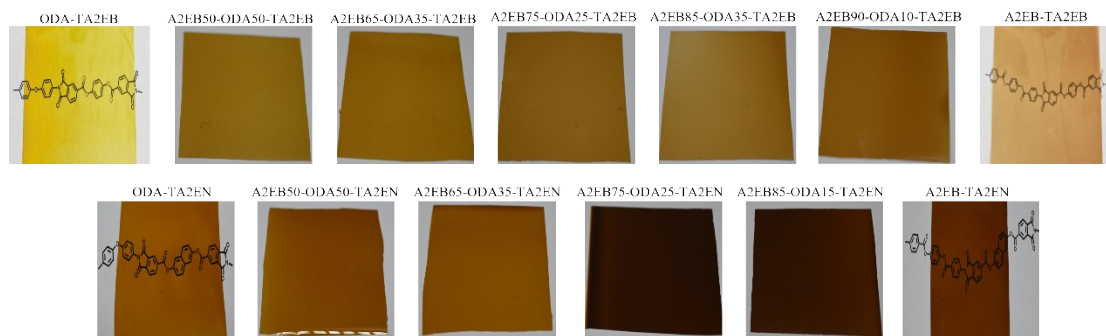
Figure S2. ^{1}H-NMR spectrum of TA2EN in DMSO-d_6.

Figure S3. The images of PEsEtI films.
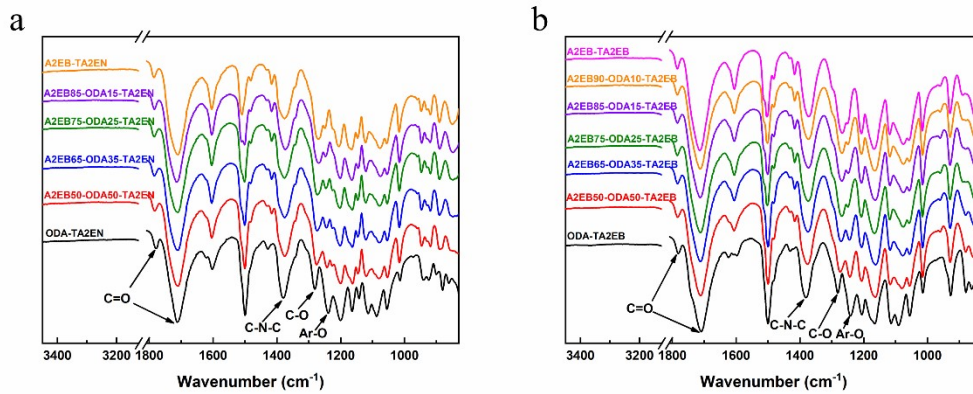
Figure S4. FTIR spectra of A2EB-ODA-TA2EN (a) and A2EB-ODA-TA2EB (b).
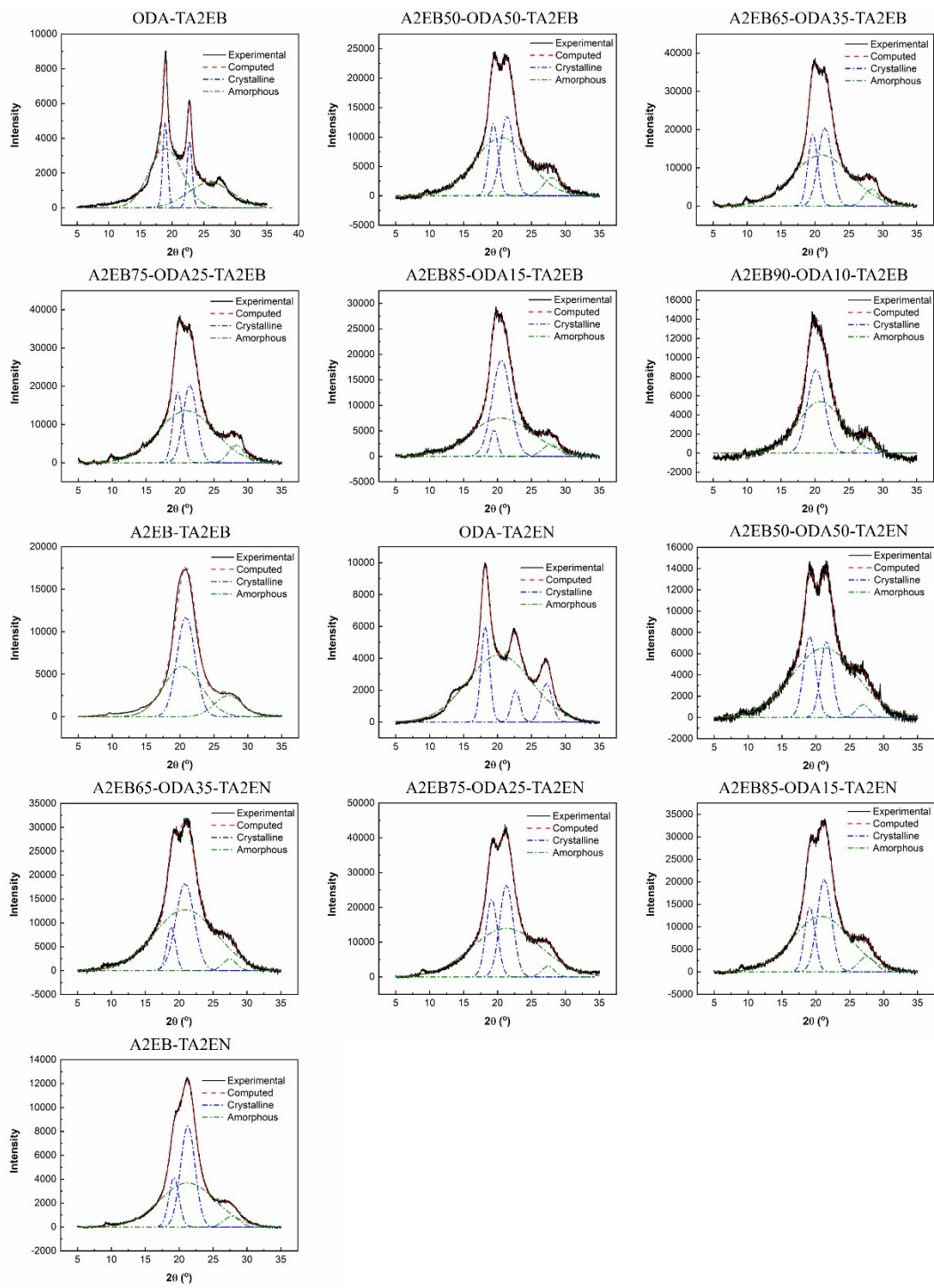
Figure S5. Peak fitting of PEsEtIs.
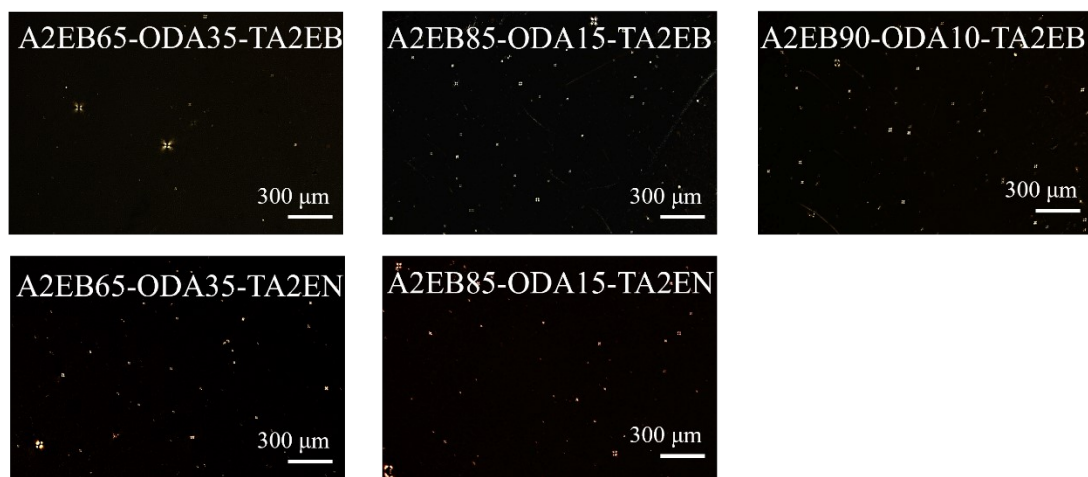
Figure S6. The POM images of PEsEtIs.
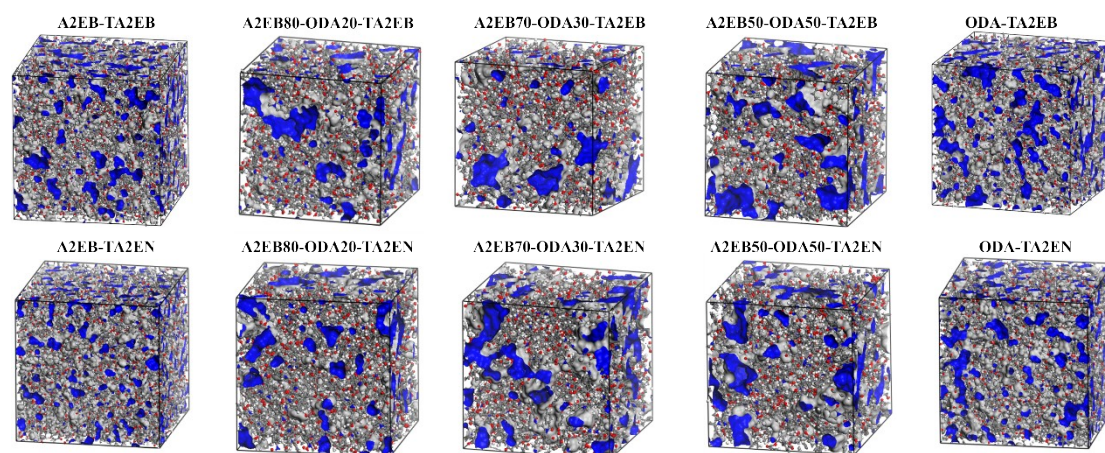
Figure S7. Three-dimensional periodic boundary cells of PEsEtI films (gray part represents the molecule chain skeleton while blue part represents the free volume).
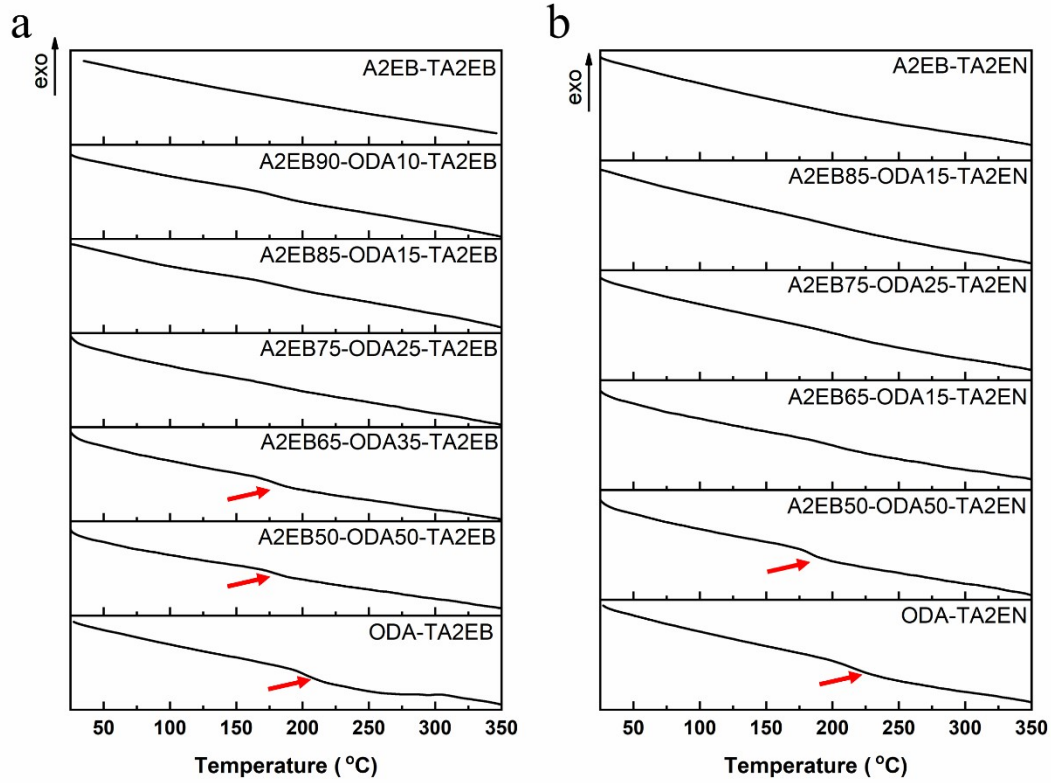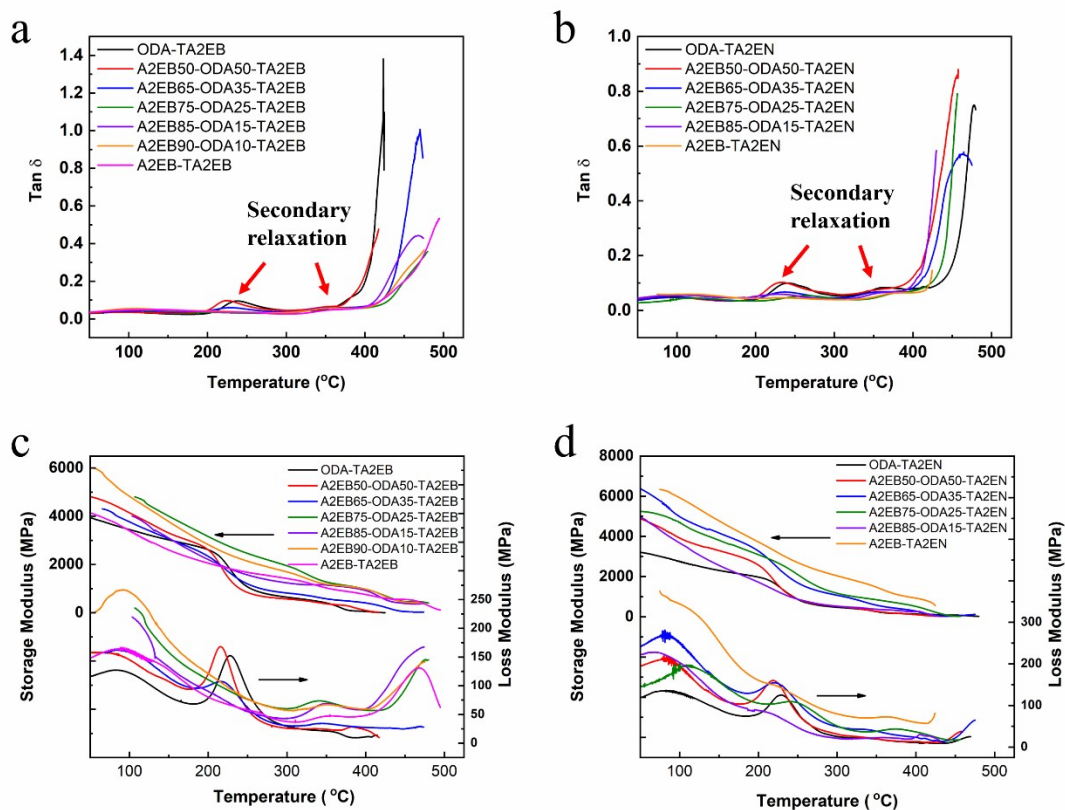
Figure S8. DSC curves of PEsEtIs.

Figure S9. DMA curves of PEsEtIs.

All PEsEtIs have secondary relaxation due to the localized motion of ester groups within the low-frequency range. The intensity of secondary relaxation decreases and the temperature increases with the decrease of ether bond, Similar to DSC (Figure S8).
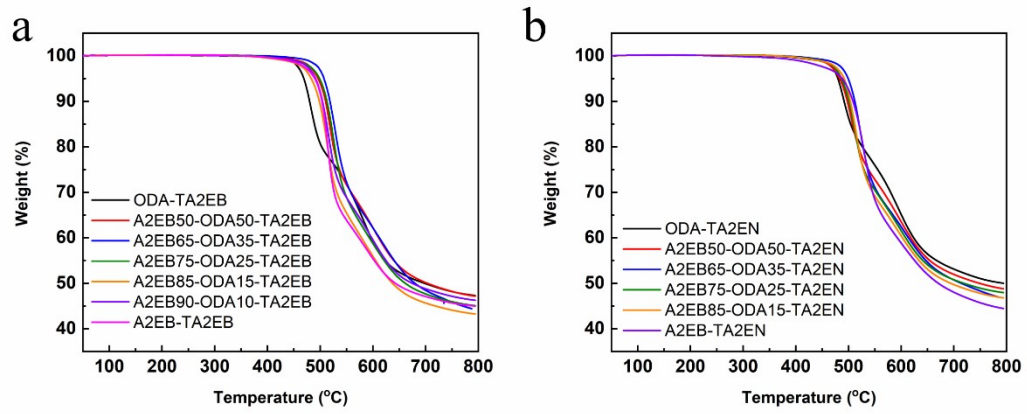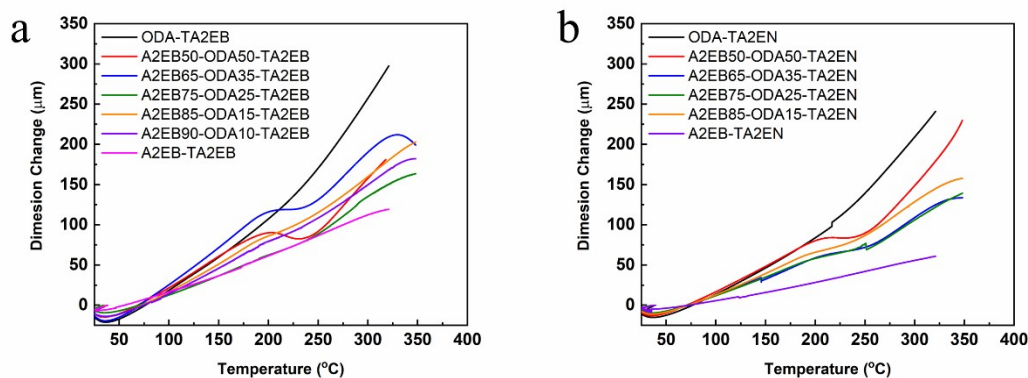
Figure S10. TGA curves of PEsEtIs.

Figure S11. TMA curves of PEsEtIs.

In the samples, TMA curves for A2EB50-ODA50-TA2EB, A2EB65-ODA35-TA2EB, A2EB50-ODA50-TA2EB, and A2EB65-ODA35-TA2EB show a platform area. This phenomenon arises because these copolymers contain two types of crystalline structures in similar proportions: one formed by A2EB-TA2EB (ether as flexible connectors) and the other by ODA-TA2EB (alternating ester-ether). The crystalline structure of A2EB-TA2EB has a lower CTE, while that of ODA-TA2EB has a higher CTE. Thus, at certain temperatures, thermal expansion in the latter crystalline structure exerts a pulling effect on the former crystalline structure, which in turn restricts the expansion of the latter crystalline structure, leading to the observed platform area.
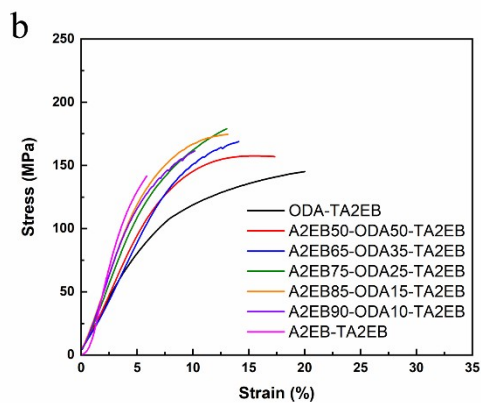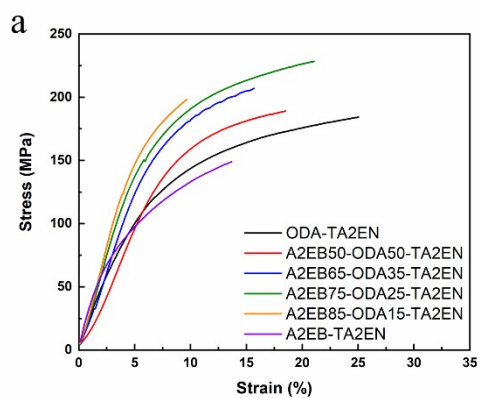
Figure S12. Stress-strain curves of PEsEtIs.

References

[1] M. Hasegawa, T. Fukuda, J. Ishii, Poly(ester imide)s with Low Linear Coefficients of Thermal Expansion and Low Water Uptake (VII): A Strategy to Achieve Ultra-Low Dissipation Factors at 10 GHz, Polymers, 16 (2024) 653.

[2] A. Eftekhari, J.S. Amin, S. Zendehboudi, A molecular dynamics approach to investigate effect of pressure on asphaltene self-aggregation, J. Mol. Liq. 376 (2023) 121347.

[3] F. Chen, F. Liu, X. Du, Molecular dynamics simulation of crosslinking process and mechanical properties of epoxy under the accelerator, J. Polym. Sci. 140 (2) (2023) e53302.

[4] H. Corneliu, I. Ronova, E. Hamciuc, M. Bruma, The effect of the rotation hindrance on physical properties of some heterocyclic polyamides containing pendent imide groups, Angew. makromol. Chem. 254 (1998) 67-74.

[5] I. Salahshoori, A. Mohseni, M. Namayandeh Jorabchi, S. Ghasemi, M. Afshar, S. Wohlrab, Study of modified PVDF membranes with high-capacity adsorption features using Quantum mechanics, Monte Carlo, and Molecular Dynamics Simulations, J. Mol. Liq. 375 (2023) 121286.

[6] M.J. Frisch, G.W. Trucks, H.B. Schlegel, G.E. Scuseria, M.A. Robb, J.R. Cheeseman, G. Scalmani, V. Barone, G.A. Petersson, H. Nakatsuji, X. Li, M. Caricato, A.V. Marenich, J. Bloino, B.G. Janesko, R. Gomperts, B. Mennucci, H.P. Hratchian, J.V. Ortiz, A.F. Izmaylov, J.L. Sonnenberg, Williams, F. Ding, F. Lipparini, F. Egidi, J. Goings, B. Peng, A. Petrone, T. Henderson, D. Ranasinghe, V.G. Zakrzewski, J. Gao, N. Rega, G. Zheng, W. Liang, M. Hada, M. Ehara, K. Toyota, R. Fukuda, J. Hasegawa, M. Ishida, T. Nakajima, Y. Honda, O. Kitao, H.

Nakai, T. Vreven, K. Throssell, J.A. Montgomery Jr., J.E. Peralta, F. Ogliaro, M.J. Bearpark,

J.J. Heyd, E.N. Brothers, K.N. Kudin, V.N. Staroverov, T.A. Keith, R. Kobayashi, J. Normand,

K. Raghavachari, A.P. Rendell, J.C. Burant, S.S. Iyengar, J. Tomasi, M. Cossi, J.M. Millam,

M. Klene, C. Adamo, R. Cammi, J.W. Ochterski, R.L. Martin, K. Morokuma, O. Farkas, J.B.

Foresman, D.J. Fox.

[7] G. Buemi, R. Sergio Cataliotti, The Polarizable continuum potential model in the liquid state

Calculations. Density functional computational analysis of the anharmonic vibrational spectrum

of liquid water, J. Mol. Liq. 340 (2021) 116941.

[8] A.D. Becke, Density-functional exchange-energy approximation with correct asymptotic

behavior, Phys. Rev. A 38 (6) (1988) 3098-3100.

[9] A.D. Becke, Density-functional thermochemistry. I. The effect of the exchange-only gradient

correction, J. Chem. Phys. 96 (3) (1992) 2155-2160.

[10] J.-J. Liu, J.-H. Tan, Y. Zeng, Y.-W. Liu, K.-J. Zeng, Y.-J. Liu, R.-M. Wu, H. Chen, Synthesis

and characterization of high-barrier polyimide containing rigid planar moieties and amide

groups, Polym. Test. 61 (2017) 83-92.

[11] Z. Yang, P. Ma, F. Li, H. Guo, C. Kang, L. Gao, Ultrahigh thermal-stability polyimides with

low CTE and required flexibility by formation of hydrogen bonds between poly(amic acid)s,

Eur. Polym. J. 148 (2021) 110369.

[12] P. Yuan, F. Annabi-Bergaya, Q. Tao, M. Fan, Z. Liu, J. Zhu, H. He, T. Chen, A combined

study by XRD, FTIR, TG and HRTEM on the structure of delaminated Fe-intercalated/pillared

clay, J. Colloid Interface Sci. 324 (1) (2008) 142-149.

[13] R. Sengupta, V.K. Tikku, A.K. Somani, T.K. Chaki, A.K. Bhowmick, Electron beam irradiated

polyamide-6,6 films-I: characterization by wide angle X-ray scattering and infrared spectroscopy, Radiat. Phys. Chem. 72 (5) (2005) 625-633.

[14] T. Lu, C. Chen, Uncertainty evaluation of humidity sensors calibrated by saturated salt solutions, Measurement 40 (6) (2007) 591-599.

[15] A. Carotenuto, M. Dell'Isola, An experimental verification of saturated salt solution-based humidity fixed points, Int. J. Thermophys. 17 (1996) 1423-1439.